Paper 243

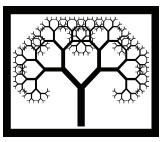

Proceedings of the Ninth International Conference
on Computational Structures Technology,
B.H.V. Topping and M. Papadrakakis, (Editors),
Civil-Comp Press, Stirlingshire, Scotland

Practical Aspects Concerning the Numerical Implementation of the Fatigue Growth of Curved Cracks

M.A. Meggiolaro[1], A.C.O. Miranda[2], L.F. Martha[2] and J.T.P. Castro[1]
[1] Mechanical Engineering Department
[2] Civil Engineering Department
Pontifical Catholic University of Rio de Janeiro, Brazil

Abstract

The theory required to predict the two-dimensional propagation path of cracks under general bi-axial loading is well known, however its implementation in an efficient and reliable computational code is a far from trivial task. The purpose of this work is to describe how the difficulties involved in translating such theoretical tools into practical numerical techniques have been solved, as well as how these techniques were used in a successful special-purpose academic program called **Quebra2D**. Experiments on modified C(T) specimens made out of 1020 steel are used to validate the accuracy of the numerical predictions obtained from the presented approach.

Keywords: curved cracks, crack path prediction, computational fracture mechanics, finite elements, meshing algorithm, equivalent stress intensity factors.

1 Introduction

It is almost invariably necessary to use computational methods to predict the generally curved crack path and its associated stress intensity factors (SIF) in real components. Several methods have been proposed to numerically compute such SIF and crack growth directions [1].

The most popular methods to computationally obtain the SIF are the displacement correlation technique (DCT), the potential energy release rate computed by means of a modified crack-closure integral technique (MCC), and the J-integral computed by means of the equivalent domain integral (EDI). Several models have also been proposed to obtain the equivalent SIF used to treat the 2D fatigue crack growth problem under general bi-axial loading. These models are based, e.g., on the displacements behind the crack tip reaching a critical value, or on the relations between the potential energy release rate and the SIF.

The numerical computation of the crack incremental direction in the linear-elastic regime is, in general, based on one of the three most used criteria: the maximum circumferential stress, the maximum potential energy release rate, and the

minimum strain energy density. The computed values at each calculation step are used to obtain the crack incremental growth direction - and thus the fatigue crack path - in the linear-elastic regime.

In this work, the above methods are reviewed, together with details on their implementation in a computational code called **Quebra2D**. The crack representation scheme used in **Quebra2D** is based on the discrete approach. In this sense, the program is similar to well-known 2D simulators, such as Franc2D [1] for example. This program includes all methods described above to compute the crack increment direction and the associated stress-intensity factors along the crack path. Moreover, its adaptive FE analyses are coupled with modern and very efficient automatic remeshing schemes, which substantially decrease the computational effort.

The computational methods to obtain the SIF and crack growth direction are detailed next.

2 Numerical Computation of Stress-Intensity Factors

According to Bittencourt et al. [1], three methods can be chosen to compute the stress-intensity factors (*SIF*) along the generally curved crack path in 2D finite element models: the displacement correlation technique (*DCT*) [2], the potential energy release rate computed by means of a modified crack-closure integral technique (*MCC*) [3, 4], and the *J*-integral computed by means of the equivalent domain integral (*EDI*) together with a mode decomposition scheme [5].

An important detail necessary to compute the *SIF* using the *DCT* is to transform the nodal displacements from a global *XY* coordinate system into a local *xy* system aligned with the last crack increment. This increment, in general, makes an angle α with the *X* axis, see Figure 1. Using the well-known equations for quarter-point singular triangular elements [6], Mode I and Mode II SIF can be evaluated in the local *xy* system by

$$K_I = \left(\frac{\mu}{\kappa+1}\right)\sqrt{\frac{2\pi}{L}}\left(4v_{j-1} - v_{j-2}\right)$$
$$K_{II} = \left(\frac{\mu}{\kappa+1}\right)\sqrt{\frac{2\pi}{L}}\left(4u_{j-1} - u_{j-2}\right) \quad (1)$$

where $\kappa = 3 - 4\nu$ for plane strain, $\kappa = (3 - \nu)/(1 + \nu)$ for plane stress, ν is the Poisson ratio, μ is the shear modulus, v_{j-1} and v_{j-2} are the relative displacements in the *y* local coordinate system direction at the *j–1* and *j–2* nodes, u_{j-1} and u_{j-2} are the relative displacements in the *x* local coordinate system direction at the *j–1* and *j–2* nodes, and *L* is the element size.

The *MCC* method is based on Irwin's crack-closure integral concept. Rybicki and Kanninen [3] were the first to use this approach with a single finite element analysis, and Raju [4] proposed simplified expressions for singularity elements. However, the numerical computation of G_I and G_{II}, the strain-energy release rates, originally proposed by Raju to unit thickness, $t = 1$, should be generalized to take into account a different thickness. In this case, the components G_I and G_{II} for pure Mode I and Mode II, and for mixed mode conditions are given as

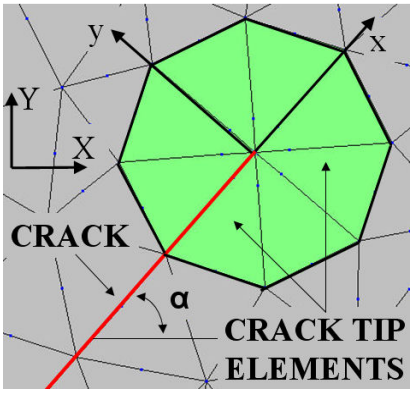

(a)

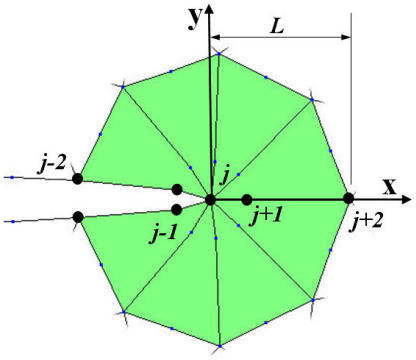

(b)

Figure 1: Crack tip elements in a: (a) global coordinate system and (b) local coordinate system.

$$G_I = -\frac{1}{2Lt}\left[F_{y_i}\left\{t_{11}\left(v_m - v_{m'}\right) + t_{12}\left(v_l - v_{l'}\right)\right\} + F_{y_j}\left\{t_{21}\left(v_m - v_{m'}\right) + t_{22}\left(v_l - v_{l'}\right)\right\}\right]$$
$$G_{II} = -\frac{1}{2Lt}\left[F_{x_i}\left\{t_{11}\left(u_m - u_{m'}\right) + t_{12}\left(u_l - u_{l'}\right)\right\} + F_{x_j}\left\{t_{21}\left(u_m - u_{m'}\right) + t_{22}\left(u_l - u_{l'}\right)\right\}\right] \quad (2)$$

where F_{xi}, F_{xj}, F_{yi}, and F_{yj} are the consistent nodal forces acting on nodes i and j in the x and y directions of the local coordinate system in Figure 1(b); u and v are the nodal displacements at the m, m', l and l' nodes in the x and y directions, respectively (see Figure 2); and $t_{11} = 6 - 3\pi/2$, $t_{12} = 6\pi - 20$, $t_{21} = 1/2$, and $t_{22} = 1$.

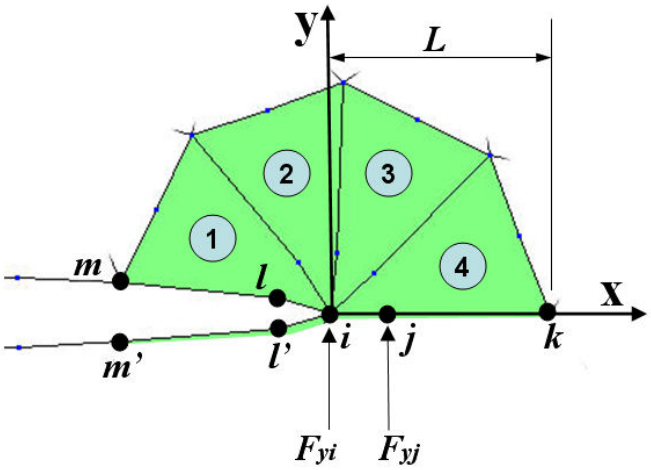

Figure 2: Nodes at crack tip elements and consistent nodal forces ahead of the crack tip.

The nodal forces F_{xi} and F_{yi} are computed from elements 1, 2, 3 and 4, but the forces F_{xj} and F_{yj} are computed from element 4 only. Under linear elastic conditions (LEFM), the stress-intensity factors are related to the energy release rates by

$$G_I = \frac{\kappa+1}{8\mu}K_I^2 \quad \text{and} \quad G_{II} = \frac{\kappa+1}{8\mu}K_{II}^2 \quad (3)$$

where κ has been previously defined for plane stress and plane strain conditions. It is assumed that the classical ASTM E399 requirements for validating a K_{IC} toughness test can also be used in fatigue crack growth to characterize plane strain conditions.

The J-integral is a path independent contour integral introduced by Rice [7] to study non-linear elastic materials under small scale yielding. The equivalent domain integral method replaces the integration along the contour by another one over a finite size domain, using the divergence theorem. This definition is more convenient for finite element analysis. For two-dimensional problems, the contour integral is replaced by an area integral

$$J = -\int_A \left[W \frac{\partial q}{\partial x} - \sigma_{ij} \frac{\partial u_i}{\partial x} \frac{\partial q}{\partial x} \right] dA - \int_A \left\{ \frac{\partial W}{\partial x} - \frac{\partial}{\partial x} \left[\sigma_{ij} \frac{\partial u_i}{\partial x} \right] \right\} q dA - \int_S t_i \frac{\partial u_i}{\partial x} q ds \tag{4}$$

where W is the strain energy density; q is a continuous function that allows for the equivalent domain integral to be treated in the finite element formulation; σ_{ij} are the stresses at the contour C, which is any path surrounding the crack tip; u_i are the displacements correspondent to local i-axes; t_i is the crack face pressure load, and s is the arc length of the contour. Usually, a linear function is chosen for q, which assumes a unit value at the crack tip and a null value along the contour. For linear-elastic materials, the second term in Equation 4 vanishes. The third term will vanish if the crack faces are not loaded, or if $q = 0$ at the loaded portions of the crack faces.

3 Computation of the Crack Increment Direction

In 2D finite element analysis, the three most used criteria for numeric computation of crack (incremental) growth in the linear-elastic regime are: (a) the maximum circumferential stress ($\sigma_{\theta max}$) [8], (b) the maximum potential energy release rate ($G_{\theta max}$) [9], and (c) the minimum strain energy density ($S_{\theta min}$) [10].

In the first criterion, Erdogan and Sih considered that the crack extension should occur in the direction that maximizes the circumferential stress in the region close to the crack tip [8]. In the second, Hussain et al. [9] have suggested that the crack extension occurs in the direction that causes the maximum fracturing energy release rate. And in the last, Sih [10] assumed that the crack growth direction is determined by the minimum strain energy density value near the crack tip. Bittencourt et al. [1] claimed that, if the crack orientation is allowed to change in automatic fracture simulation, the three criteria give basically the same results. However, there are few results to support Bittencourt's affirmation.

The stresses on the crack tip for Modes I and II are given by summing up the stresses obtained for each mode separately [11]. As a result, the following equations are obtained in polar coordinates

$$\sigma_r = \frac{1}{\sqrt{2\pi r}} \cos(\theta/2) \left\{ K_I \left[1 + \sin^2(\theta/2) \right] + \frac{3}{2} K_{II} \sin\theta - 2 K_{II} \tan(\theta/2) \right\} \tag{5}$$

$$\sigma_\theta = \frac{1}{\sqrt{2\pi r}} cos(\theta/2)\left[K_I cos^2(\theta/2) - \frac{3}{2} K_{II}\, sin\,\theta \right] \tag{6}$$

$$\tau_{r\theta} = \frac{1}{\sqrt{2\pi r}} cos(\theta/2)\left[K_I\, sin\,\theta + K_{II}\left(3cos\,\theta - 1\right)\right] \tag{7}$$

These expressions are valid both for plane stress and plane strain. The maximum circumferential stress criterion determines that the crack extension begins on a plane perpendicular to the direction in which σ_θ is maximum, thus $\tau_{r\theta} = 0$. It also states that the monotonic (non-fatigued) extension shall occur when $\sigma_{\theta max}$ reaches a critical value corresponding to a property of the material (K_{IC} for Mode I). From Equations (5-7) and $\tau_{r\theta} = 0$, a trivial solution $\theta = \pm\pi$ for $cos(\theta/2) = 0$ is found, and a non-trivial solution is given by

$$K_I sin\,\theta + K_{II}(3cos\,\theta - 1) = 0 \tag{8}$$

It is found that, for pure Mode I, $K_{II} = 0$, $K_I\, sin\,\theta = 0$, and $\theta = 0°$, and for pure Mode II that $K_I = 0$, $K_{II}\,(3cos\,\theta - 1) = 0$, and $\theta = \pm 75°$. These θ are the extreme values of the crack propagation angle. The intermediate values are found solving Equation (8) for θ considering mixed mode, resulting in

$$\theta = 2\,arctan\left(\frac{1}{4}\frac{K_I}{K_{II}} \pm \frac{1}{4}\sqrt{\left(\frac{K_I}{K_{II}}\right)^2 + 8} \right) \tag{9}$$

where the sign of θ is the opposite of the sign of K_{II}.

Hussain et al. [9] used complex variable mapping functions to obtain the strain energy release rate G at a direction θ with respect to the crack propagation plane under Mode I and II combined loading. They assumed that crack extension occurs in a direction $\theta = \theta_0$ that maximizes G, leading to the maximum fracturing energy release rate (G_{max}) criterion:

$$G(\theta) = \frac{4}{E}\left(\frac{1}{3+cos^2\theta}\right)^2 \left(\frac{1-\theta/\pi}{1+\theta/\pi}\right)^{\theta/\pi} \left[\left(1+3cos^2\theta\right)K_I^2 + 8\,sin\,\theta\,cos\,\theta\cdot K_I K_{II} + \left(9-5cos^2\theta\right)K_{II}^2\right] \tag{10}$$

In this work, to find the angle that maximizes the energy release rate, algorithm codes from [12] are adopted. First, the derivative function $dG(\theta)/d\theta = 0$ is obtained from Equation (9). Then, two simple routines from [12] are used to obtain the correct value of the crack propagation angle: (a) *zbrac* – to expand an initial guessed range θ_1 to θ_2 geometrically until a root is bracketed by the returned values θ_1 and θ_2; (b) rtbis – to find the root of a function using bisection given the function and the initial range θ_1 and θ_2. The guess values to the *sbrac* routine are obtained from Equation (9) and considering a tolerance.

Sih [13] proposed a criterion for mixed-mode loading based on the strain energy density S around the crack tip. It is assumed that the crack propagates in a direction θ that minimizes S, defined as

$$\begin{aligned} a_{11} &= \frac{1}{16\mu}\left[\left(\kappa-\cos\theta\right)\left(1+\cos\theta\right)\right] \\ a_{12} &= \frac{1}{16\mu}\sin\theta\left[2\cos\theta-\left(\kappa-1\right)\right] \\ a_{22} &= \frac{1}{16\mu}\left[\left(\kappa+1\right)\left(1-\cos\theta\right)+\left(3\cos\theta-1\right)\left(1+\cos\theta\right)\right] \\ S\left(\theta\right) &= a_{11}K_I^2+2a_{12}K_IK_{II}+a_{22}K_{II}^2 \end{aligned} \tag{11}$$

The same process used to maximize the energy release rate can be employed to calculate the value of the crack propagation angle. To do that, it is sufficient to obtain the derivative function $dS\left(\theta\right)/d\theta=0$, resulting in

$$\begin{aligned} \frac{da_{11}}{d\theta} &= \frac{1}{16\mu}\sin\theta\left[\left(1+\cos\theta\right)-\left(\kappa-\cos\theta\right)\right] \\ \frac{da_{12}}{d\theta} &= \frac{1}{16\mu}\left[\cos\theta\left(2\cos\theta-\kappa+1\right)-2\left(\sin\theta\right)^2\right] \\ \frac{da_{22}}{d\theta} &= \frac{1}{16\mu}\left[\left(\kappa+1\right)\sin\theta-3\sin\theta\left(1+\cos\theta\right)-\left(3\cos\theta-1\right)\sin\theta\right] \\ \frac{dS\left(\theta\right)}{d\theta} &= \frac{da_{11}}{d\theta}K_I^2+2\frac{da_{12}}{d\theta}K_IK_{II}+\frac{da_{22}}{d\theta}K_{II}^2=0 \end{aligned} \tag{12}$$

4 Mixed-Mode Crack Growth Calculations

The calculated Mode I and II SIF K_I and K_{II} are now used to obtain an equivalent SIF K_{eq}. The fatigue crack growth rate can then be computed from the equivalent stress intensity range ΔK_{eq} by a simple McEvily-type model [13]:

$$\frac{da}{dN}=A\cdot\left(\Delta K_{eq}-\Delta K_{th}\right)^m \tag{13}$$

where ΔK_{th} is the threshold SIF and A and m are the conventional tensile crack growth rate parameters for the given material. An alternative Elber-type equation can be used based on the maximum equivalent stress intensity K_{eq} and on the crack opening value K_{op}, namely

$$\frac{da}{dN}=A\cdot\left(K_{eq}-K_{op}\right)^m \tag{14}$$

Several models have been proposed to obtain K_{eq} from K_I and K_{II} (and K_{III}, when it is important). E.g., Tanaka [14] obtained an equivalent stress intensity model based on the displacements behind the crack tip reaching a critical value, leading to

$$K_{eq} = \left[K_I^4 + 8 \cdot K_{II}^4 + \frac{8 \cdot K_{III}^4}{1 - \nu} \right]^{1/4} \tag{15}$$

where ν is Poisson's coefficient.

Another expression for K_{eq} can be derived for elastic loading under plane stress conditions, based on the relations between the potential energy release rate G and the SIF [15], leading to

$$K_{eq} = \sqrt{K_I^2 + K_{II}^2 + (1+\nu) \cdot K_{III}^2} \tag{16}$$

From Equation (10), an equivalent SIF is obtained at $\theta = \theta_0$ that maximizes the expression

$$K_{eq} = \sqrt{\frac{4}{(3+\cos^2\theta)^2} \left(\frac{1-\theta/\pi}{1+\theta/\pi} \right)^{\theta/\pi} [(1+3\cos^2\theta) K_I^2 + 8 \sin\theta \cos\theta \cdot K_I K_{II} + (9-5\cos^2\theta) K_{II}^2]} \tag{17}$$

Such computed θ_0 values at each calculation step are used to obtain the crack incremental growth direction - and thus the fatigue crack path - in the linear-elastic regime.

From Equation (11), the associated equivalent SIF is then calculated at $\theta = \theta_0'$ that minimizes the expression

$$K_{eq} = \sqrt{a_{11} K_I^2 + 2 a_{12} K_I K_{II} + a_{22} K_{II}^2} \tag{18}$$

And from Equations (5-9), according to the $\sigma_{\theta max}$ criterion, the equivalent SIF is calculated at the value $\theta = \theta_0''$, which maximizes the expression

$$K_{eq} = \frac{1}{4} \left(3 \cos\frac{\theta}{2} + \cos\frac{3\theta}{2} \right) \cdot K_I - \frac{3}{4} \left(\sin\frac{\theta}{2} + \sin\frac{3\theta}{2} \right) \cdot K_{II} \tag{19}$$

Several other criteria have been proposed in the literature, such as the ones by Nuismer, Amestoy et al., Richard, Schöllmann et al., and Pook [16]. A few of these criteria even predict the warping angle of a 3-D crack subject to Mode III loading. A comprehensive review of the proposed equivalent SIF and propagation angle expressions can be found in [16].

All presented models have notable differences if the amount of Mode II loading is significant. For instance, under pure Mode II loading, the propagation angle θ is

±70.5°, ±75° and ±82° according to the $\sigma_{\theta max}$, $\mathcal{G}_{max}$ and S_{min} models, respectively, leading to K_{eq} values of approximately $1.15 \cdot K_{II}$, $1.60 \cdot K_{II}$ and $1.05 \cdot K_{II}$ (assuming ν = 0.3). In addition, Tanaka's model results in this case in $K_{eq} = 1.68 \cdot K_{II}$, while Equation (4) furnishes $K_{eq} = K_{II}$. The values of θ and K_{eq} obtained from each model are plotted in Figures 3 and 4 as a function of the K_{II}/K_I ratio.

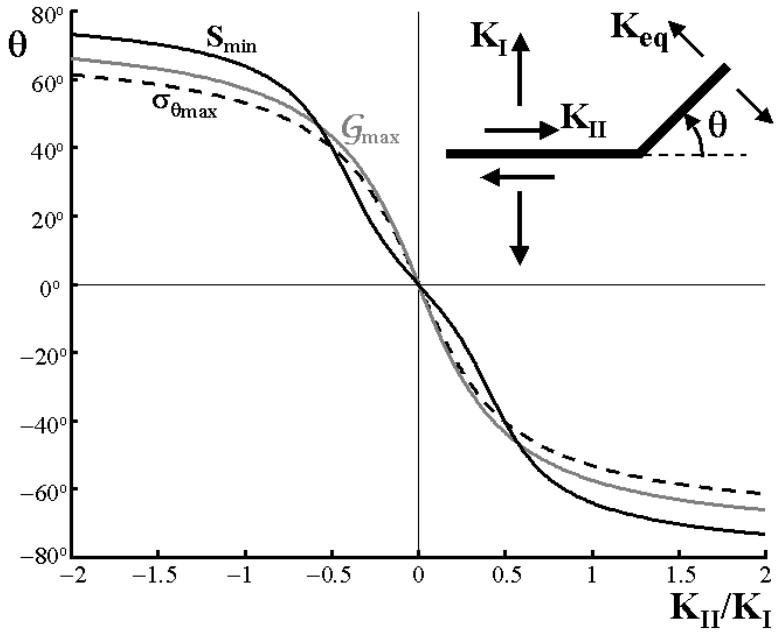

Figure 3: Crack propagation direction θ as a function of the K_{II}/K_I ratio according to the $\sigma_{\theta max}$, G$_{max}$ and S_{min} models.

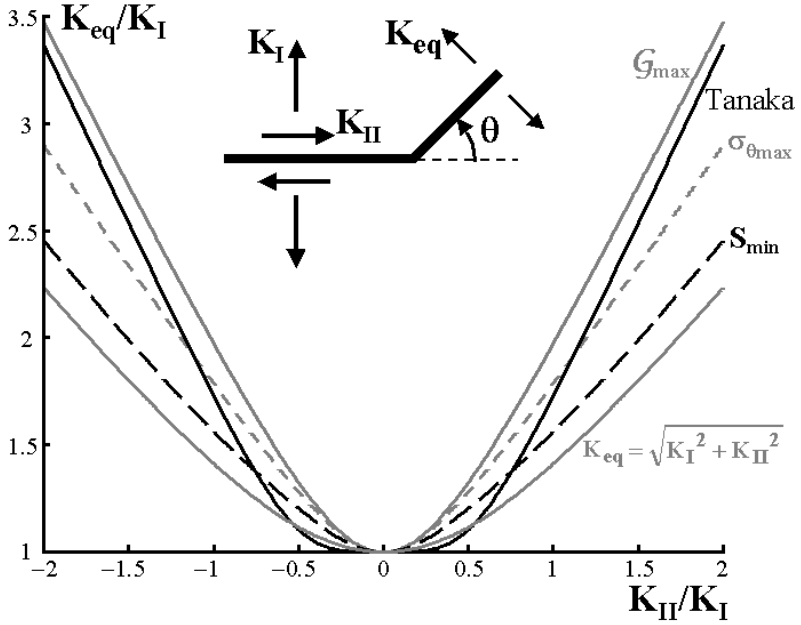

Figure 4: Equivalent SIF K_{eq} as a function of the K_{II}/K_I ratio according to several models.

The differences among the studied models might be significant for mixed-mode fracture predictions, however they turn out to be negligible for fatigue crack propagation calculations. In fact, since all above models predict crack path deviation ($\theta \neq 0$) under any K_{II} different than zero (see Figure 4), they imply that fatigue cracks will always attempt to propagate in pure Mode I, minimizing the amount of Mode II loading, curving their paths if necessary to avoid rubbing their faces. As soon as the crack path is curved to follow pure Mode I, all models agree that K_{eq} is equal to K_I. Therefore, for sufficiently refined meshes, all above models should result in approximately the same crack path.

5 Experimental Verification of the Crack Path Prediction

Fatigue crack growth experiments are performed on C(T) specimens of cold-rolled AISI 1020 steel, with yield strength S_Y = 285MPa, ultimate strength S_U = 491MPa, Young modulus E = 205GPa, and reduction in area RA = 54%, measured according to the ASTM E 8M-99 standard. The analyzed weight percent composition of this steel is: 0.19C, 0.46Mn, 0.14Si, 0.11Cu, 0.052Ni, 0.045Cr, 0.007Mo, 0.002Nb, 0.002Ti, Fe balance.

The fatigue crack propagation tests are performed in a 250kN computer-controlled servo-hydraulic testing machine, at two $R = K_{min}/K_{max}$ ratios, namely R = 0.1 and R = 0.7. The crack length is measured following ASTM E 647-99 procedures. The measured growth rates on 16 standard compact tension C(T) test specimens are fitted by a modified McEvily da/dN equation (in m/cycle), as shown in Equation (20), where the propagation threshold under R = 0 is ΔK_0 = 11.5 MPa√m, and the fracture toughness is K_C = 280 MPa√m.

$$\frac{da}{dN} = 2.5 \cdot 10^{-10} \cdot \left[\Delta K - 11.5 \cdot (1 - 0.55 \cdot R)\right]^{2.2} \tag{20}$$

Three modified C(T) specimens have been designed and tested to verify the crack path predictions width w = 29.5mm and thickness t = 8mm, but each one with a 7mm-diameter hole positioned at a slightly different horizontal distance A and vertical distance B from the notch root, as shown in Figure 5. A larger fourth specimen with w = 50mm and t = 10mm was also tested, see Figure 5.

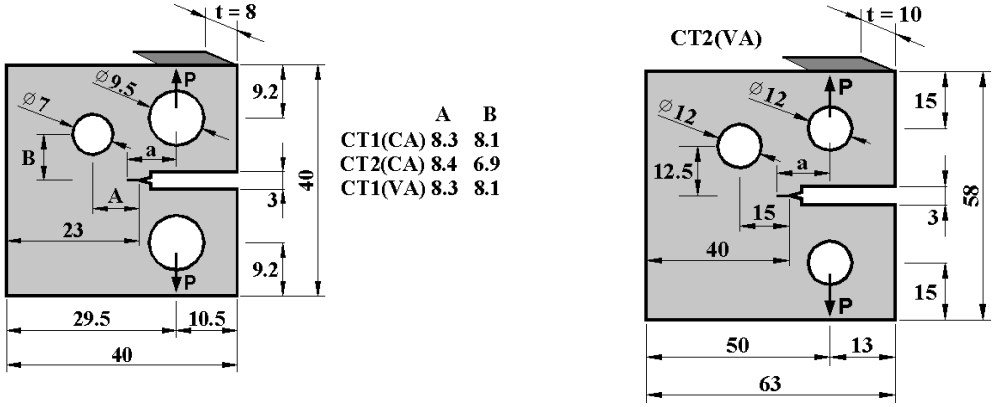

Figure 5: Measured dimensions of the hole-modified C(T) specimens (mm).

Two very different crack growth behaviours had been predicted by the FE modelling of the C(T) specimens, depending on the hole position. The predictions indicated that the fatigue crack was always attracted by the hole, but it could either curve its path and grow toward the hole ("sink in the hole" behaviour) or just be deflected by the hole and continue to propagate after missing it ("miss the hole" behaviour).

Using the **Quebra2D** program, the transition point between the "sink in the hole" and the "miss the hole" crack growth behaviours was identified. The three modified C(T) specimens were designed so that specimens named CT1(CA) and CT1(VA) had the hole just half a mm above the transition point, and a specimen named CT2(CA) had the hole half a mm below it. The chosen specimen geometries were machined, measured, and FE remodelled, to account for small deviations in the machining process. In this way, it could be assured that the numerical models used in the predictions reproduced the real geometry of the tested specimens.

Specimens CT1(CA) and CT2(CA) were tested under constant amplitude (CA) loading, under a quasi-constant stress-intensity range $\Delta K_I \cong 20\text{MPa}\sqrt{\text{m}}$ and load ratio $R = 0.1$. The holed CT1(VA) specimen was tested under VA loading.

Figure 6 shows the predicted and measured crack paths for the three modified specimens (in mm) under CA or VA loading, presenting a very good match. This suggests that the curved crack paths predicted under CA loading give good estimates of the measured paths under either CA or VA loading.

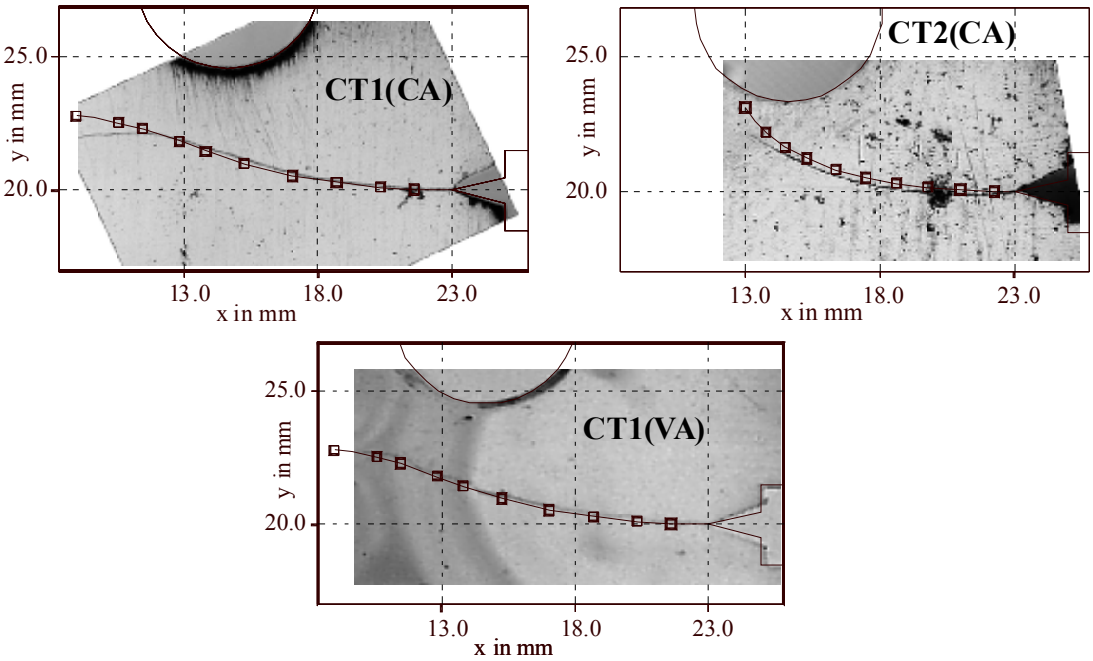

Figure 6: Predicted and measured crack paths for the modified C(T) specimens (mm).

6 Conclusions

In this work, the main methods to predict the path and stress intensity factors of fatigue cracks were reviewed. Details on their implementation in a computational code called **Quebra2D** were presented. Experimental results were used to verify the accuracy of the numerical predictions. The results showed that the implemented computational code was able to predict the curved crack path in all experiments, either under constant or variable amplitude loading.

References

[1] T.N. Bittencourt, A. Barry, A.R. Ingraffea, "Comparison of mixed-mode stress-intensity factors obtained through displacement correlation, J-integral formulation, and modified crack-closure integral," *Fatigue and Fracture Mechanics*: 22nd Volume, *ASTM - Standard Technical Publication (STP)* 1131: 69-82, ISBN: 0-8031-1440-0, 1992.

[2] C.F. Shih, H.G. de Lorenzi, M.D. German, "Crack Extension Modeling with Singular Quadratic Isoparametric Elements," *International Journal of Fracture*, 12, 647-651, 1976.

[3] E.F. Rybicki, M.F. Kanninen, "A Finite Element Calculation of Stress-Intensity Factors by a Modified Crack Closure Integral," *Engineering Fracture Mechanics*, 9, 931-938, 1977.

[4] I.S. Raju, "Calculation of Strain-Energy Release Rates with Higher Order and Singular Finite Elements," *Engineering Fracture Mechanics*, 28, 251-274, 1987.

[5] H.D. Bui, "Associated Path Independent J-Integrals for Separating Mixed Modes," *Journal of Mechanics & Physics Solids*, 31, 439-448, 1983.

[6] R.S. Barsoum, "On the Use of Isoparametric Finite Elements in Linear Fracture Mechanics," *International Journal for Numerical Methods in Engineering*, 10, 25-37, 1976.

[7] J.R. Rice, "A Path Independent Integral and the Approximate Analysis of Strain Concentration by Notches and Cracks," *Journal of Applied Mechanics*, 35, 379-386, 1968.

[8] F. Erdogan, G.C. Sih, "On the Crack Extension in Plates under Plane Loading and Transverse Shear," *Journal of Basic Engineering*, 85, 519-527, 1963.

[9] M.A. Hussain, S.U. Pu, J. Underwood, "Strain Energy Release Rate for a Crack under Combined Mode I and II," *ASTM STP 560*, 2-28, 1974.

[10] G.C. Sih, "Strain-Energy-Density Factor Applied to Mixed Mode Crack Problems," *International Journal of Fracture Mechanics*, 10, 305-321, 1974.

[11] J.M. Barsom, S.T. Rolfe, *Fracture and Fatigue Control in Structures*, Prentice-Hall, New Jersey, 1987.

[12] W.H. Press, B.P. Flannery, S.A. Teukolsky, W.T. Vetterling, *Numerical Recipes in C: The Art of Scientific Computing*, Cambridge University Press, New York, 1997.

[13] A.J. McEvily, "Current Aspects of Fatigue". *Metal Science*, 11:274-84, 1977.

[14] K. Tanaka, “Fatigue Propagation from a Crack Inclined to the Cyclic Tensile Axis.” *Eng Fracture Mechanics*, 6:493-507, 1974.
[15] G.R. Irwin, “Analysis of Stresses and Strains Near the End of a Crack Transversing a Plate.” *J. Applied Mechanics*, 24:361-70, 1957.
[16] H.A. Richard, “Theoretical Crack Path Determination.” Int Conference on Fatigue Crack Paths, Parma, Italy, 2003.